AIAA JOURNAL
Vol. 32, No. 1, January 1994

Flow Alteration and Drag Reduction by Riblets in a Turbulent Boundary Layer

Seong-Ryong Park* and James M. Wallace†
University of Maryland, College Park, Maryland 20742

Detailed measurements with a miniature single-sensor hot-wire probe of the streamwise velocity field within a riblet groove of dimensionless size $h^+ \approx 14$ and $s^+ \approx 28$ (based on the riblet surface average friction velocity) have been made. The wall shear stress, when integrated over the riblet surface, yields about 4% drag reduction compared with a smooth surface with the same projected area. This is largely due to the greatly diminished wall shear stress near the bottom of the riblet valley. Four-sensor hot-wire probe measurements reveal that riblets significantly reduce the vertical flux of streamwise momentum within the riblet valley.

Introduction

THAT, under certain conditions, configuring the boundary beneath a turbulent flow into small grooves aligned with the mean flow direction, called riblets, will reduce viscous drag has been well documented for over a decade.[1,2] However, very few detailed measurements of the flowfield within and just above these riblet grooves have been made for the obvious reason that they are very difficult. In most laboratory air boundary layers the physical dimensions of such riblets are considerably less than 1 mm, and the velocities to be measured are extremely small. Vukoslavčević et al.[3] have, however, measured properties of the streamwise velocity field along the vertical planes of symmetry above the valley and above the peak of a triangular riblet surface in an air boundary layer at $R_\theta \approx 1.0 \times 10^3$. These measurements showed that the mean velocity gradient at the valley surface is much lower than at a comparison smooth flat plate surface for flows with the same freestream velocity. The mean velocity gradient over the peak was somewhat greater than that over the smooth surface. Vukoslavčević et al.[3] also determined that the turbulence intensity of the streamwise velocity fluctuations was greatly reduced deep in the riblet valley. The skewness and flatness factors indicated that the turbulence only rarely penetrates deep into the valley from the layers above. These measurements, however, were not made normal to or at a sufficient number of stations along the riblet wall surface to estimate whether and, if so, how drag reduction was achieved. Furthermore, no measurements of the vertical velocity fluctuations v were made, and so information about the vertical flux of streamwise momentum could only be inferred indirectly.

Chu et al.[4] and Choi et al.[5] have carried out direct numerical simulations of flow over riblet walls in channel flows. Most of the conclusions made from the laboratory experiment reported herein are qualitatively consistent with their simulation results, although there are some quantitative differences in detail, as will be discussed later when comparisons are made.

Experimental Facilities and Instrumentation

Wind Tunnel

The experiments were performed in an open-return, low-speed wind tunnel. The last 0.94 m of the lower wall of this tunnel is the test surface, where the smooth and riblet surfaces can be interchanged. The smooth surface and the peaks of the riblet surface were carefully aligned with the upstream lower wall of the tunnel test section, and a gradual transition of about 3 cm in length was made with pliable clay for the riblet surface. The boundary layer was tripped just downstream of the contraction and developed over the 8-m-long test section. The tunnel freestream speed can be varied from about 1 to ~5.5 m/s, with a freestream turbulence level of about 0.7% at the lowest speed.

For all the single-sensor experiments reported here, the freestream velocity was maintained at 1.29 m/s corresponding to a momentum thickness Reynolds number R_θ for the smooth surface of about 1.2×10^3, a Reynolds number R_τ, based on the friction velocity, $u_\tau \equiv \sqrt{\tau_w/\rho}$, and the boundary-layer thickness, δ, of 502. Here τ_w is the wall shear stress, and ρ is the fluid density. The friction velocity was 0.055 m/s, and δ was about 14.5 cm. The ratio of the smooth surface friction velocity to the freestream velocity U_∞ was 0.43, in good agreement with the tabulation of this ratio as a function of R_θ given by Blackwelder and Haritonidis.[6] The measurements were done at a location on the axis of the tunnel approximately 15 cm upstream of the tunnel exit, where no exit effects occur. Selected measurements were repeated over the riblet surface 20 cm further upstream of this location to verify that the flow had reached equilibrium conditions, which proved to be the case.

The four-sensor probe measurements were made with two different sensor wire configurations. For these measurements the freestream velocities were maintained at 2.4 and 2.9 m/s, respectively, corresponding for the smooth surface to $R_\theta \approx 2.1 \times 10^3$ and 2.5×10^3 and $R_\tau = 8.33 \times 10^2$ and 9.66×10^2. These higher speeds were needed for these more complex probes to perform satisfactorily. The corresponding friction velocities were 0.097 and 0.114 m/s, and the boundary-layer thicknesses were about 13.5 and 13.2 cm at these higher speeds.

Riblet Surface

The riblet surface, which had the same projected area as the smooth surface, was constructed with low thermal conductivity fiberglass with symmetric grooves of triangular cross section, 5 mm high and 10 mm span between the peaks, and with walls inclined at 45 deg to the horizontal. Knowledge of the friction velocity and the location of the origin of the vertical direction y is essential for the analysis of experimental data above both the smooth and riblet surfaces. The friction velocity of the smooth surface can be found directly by obtaining accurately measured velocities in the sublayer region and then determining the linear velocity gradient there. However, the velocity gradient in the direction normal to the riblet surface varies with location along the riblet wall.[3] Thus an average value $\bar{u}_{\tau_y}$ should be used. The origin of y for the smooth surface is unambiguous. However, to avoid the ambiguity of origin of y for the riblet surface and to obtain the velocity gradient at several locations along the surface, a single-sensor probe was traversed along four equally spaced lines *normal* to one riblet sidewall in the y_n direction of Fig. 1. These lines of data will be referred to as line 1 (beginning near the peak) to 4 (beginning in

Received April 4, 1992; revision received May 15, 1993; accepted for publication, June 27, 1993; presented as Paper 93-3256 at the AIAA 3rd Shear Flow Control Conference, Orlando, FL, July 7–9, 1993.

*Faculty Research Associate, Department of Mechanical Engineering.
†Professor, Department of Mechanical Engineering.

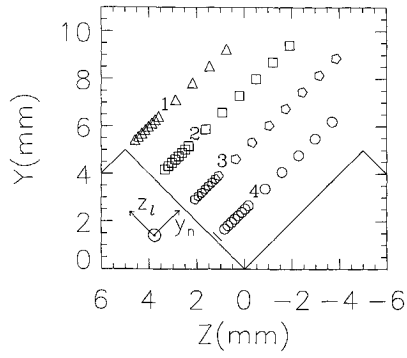

Fig. 1 Single-sensor probe locations and symbols over riblet surface. Probe length shown to scale at the base of line 4.

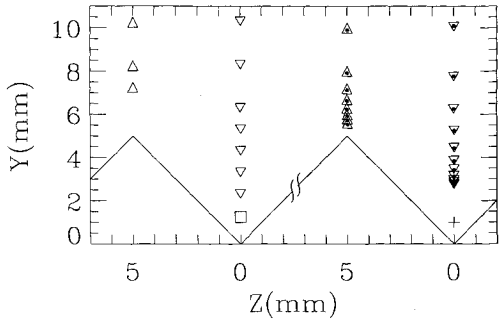

Fig. 2 Four-sensor probe locations and symbols over riblet surface. Probe size shown to scale above riblet valley: □, square-shaped probe; △, ▽, measurement locations; +, cross-shaped probe; and ▲, ▼, measurement locations.

the valley). The symbols used for these lines of data over the riblet wall in Figs. 5, 7, 9, and 11 for the single-sensor measurements are shown in Fig. 1, where the length of the sensor is also shown to scale at the base of line 4.

Four-sensor probe measurements were made by traversing the probes along lines in the planes of symmetry above the riblet peak and above the valley, respectively, as had been done with the single-sensor probe of Vukoslavčević et al.[3] The measurement locations are shown in Fig. 2, where the four-sensor probes are also indicated, to scale, at the bottom of the riblet valley. In all of the figures displaying this data and comparing it with that of others, the vertical coordinate y will be referenced to the respective surfaces: smooth, riblet peak, or riblet valley.

For the freestream velocity of 1.29 m/s and using an estimation of the smooth surface friction velocity u_τ, we first chose the normalized dimensions of the riblets to be $h^+ \approx 18$ and $s^+ \approx 36$. These were larger than the best viscous sizes for 45 deg-riblets of $h^+ \approx 9$ and $s^+ \approx 18$ found by Walsh,[7] but were still well within the range to yield net drag reduction. (A later paper by Walsh[8] indicated that these riblets might be drag neutral.) Furthermore, the average friction velocity along the riblet wall was anticipated to be smaller than the smooth surface value at this freestream speed, and so these values were considered upper bounds on the normalized height and spacing of the riblet used. After the average riblet friction velocity was found, as discussed later, the sizes, based on it, were determined to be $h^+ \approx 14$ and $s^+ \approx 28$. For the higher freestream velocities of 2.4 and 2.9 m/s, these sizes were estimated to be $h^+ \approx 23$ and 24 and $s^+ \approx 46$ and 48, i.e. outside of the drag-reducing range but still sufficiently small to demonstrate momentum flux alteration by the riblets.

Hot-Wire Probes

The single-sensor probe was of tungsten wire, approximately 0.5 mm long, with a 2.5-μm diameter, and was microwelded to the supporting prong tips. After welding, the probe tip was submerged briefly in a nickel-plating solution. This was done to make the probe robust enough so that the wire could be touched to the riblet peak, which was necessary to locate the sensor with respect to the riblet surface. The plating only reduced the sensor resistance by about 10% and only slightly reduced the frequency response of the anemometry system. The probe was calibrated in a small jet by varying the speed of its uniform flow over the range to be encountered in the experiment. Calibrations were made both before and after each boundary-layer set of measurements to check for any drift in the response of the hot-wire sensor. These calibrations were very repeatable, indicating that errors due to electronic drift and sensitivity to small ambient temperature changes were within the accuracy requirements of the experiment. To minimize these drift errors, experiments were conducted as quickly as possible and repeated three times to verify the statistical values measured. To survey locations close to the wall and to make measurements along lines normal to it, the probe was pitched down approximately 5 deg and, for the riblet surface, rolled 45 deg.

The first four-sensor probe used for the simultaneous streamwise u and vertical v fluctuating velocity component measurements was arranged so that the projection of the sensor wires on the cross-stream plane is in a square 0.5 mm on each side, as seen

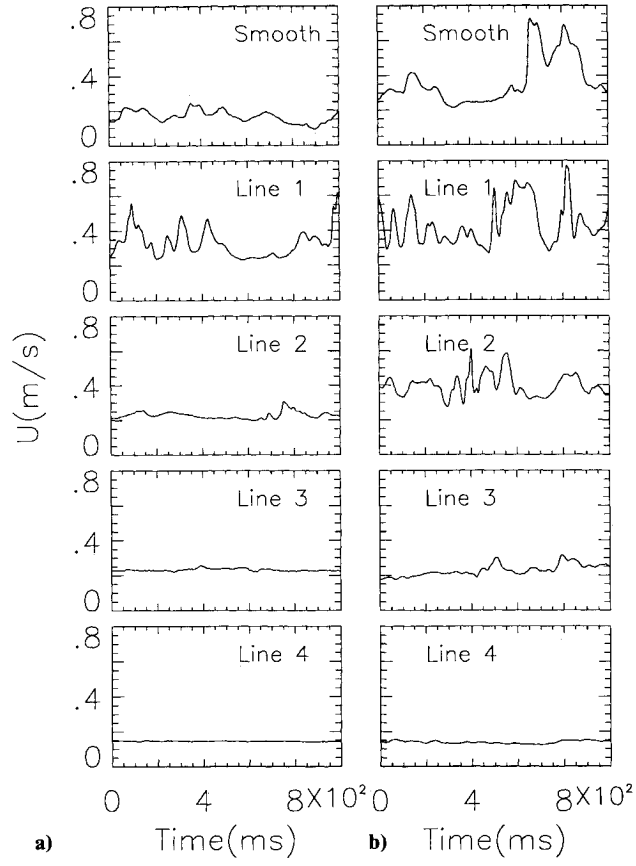

Fig. 3 Instantaneous streamwise velocity time series signals above smooth surface and at four different locations above the riblet sidewall with a single-sensor probe: a) $y_n/\delta \approx 0.004$ and b) 0.011.

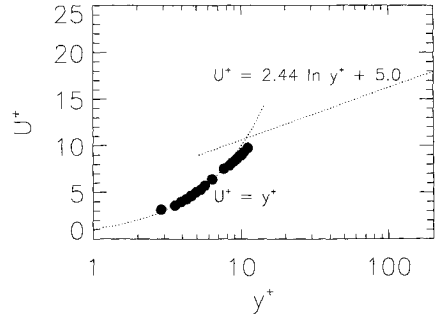

Fig. 4 Mean velocity within the viscous sublayer and buffer layer above smooth surface, normalized with the friction velocity u_τ.

in Fig. 2; thus it is, in effect, configured as two orthogonal X-arrays. Each wire was oriented at about 45 deg to the mean flow so that they were about 0.7 mm long and had 2.5-μm diameters. This four-sensor array was chosen in an attempt to also simultaneously measure the spanwise velocity fluctuations w as well as the streamwise vorticity ω_x. Park[9] describes, in detail, the operation of this probe. He found that the rms streamwise vorticity fluctuations measured with this probe were much too large, consistent with the results of Vukoslavčević and Wallace,[10] and that the mean velocity gradient adversely affected the spanwise velocity component w near the wall. Therefore, a second four-sensor array, as seen in Fig. 2, with the wires of the same dimensions but arranged in a cross-shape projection on the cross-stream plane, was used for w and a second set of u measurements. This configuration is, in effect, two orthogonal V-arrays.

Data Acquisition

The measurements were made with constant temperature AA Lab Systems hot-wire anemometer circuits. The frequency response of the anemometer system for the highest flow speeds encountered was flat up to about 5 kHz, which is much greater than the highest frequency, of about 500 Hz, at which there is any significant energy in the flow at the operating speeds investigated. Output signals of the probe were digitized at a rate of 1000 Hz, and continuous sample lengths were obtained for 180 s for the four-sensor hot-wire probe data and for 90 s for the single-sensor hot-wire probe data.

To make the measurements as close to the wall as possible and to minimize wall proximity effects such as free convection, sensors were operated in the viscous sublayer with a very low temperature overheat ratio of 1.1. Above the viscous sublayer, an overheat ratio of 1.2 was used. When the bridge is operated at such low overheat ratios, the voltage outputs of the anemometer circuits are especially sensitive to any temperature variations in the flow. For all of the data reported here, the temperature never varied more than 0.2°C over the course of the entire experiment; the high degree of repeatability of the calibrations before and after the turbulent flow data acquisition demonstrated that these temperature changes were acceptably small. The data were acquired with a 12-bit DATA Translation simultaneous sample and hold A/D converter operated by a DEC LSI 11/21 microprocessor and stored on a hard disk, before being transferred to the disk of a Sun 3/260 minicomputer for postprocessing.

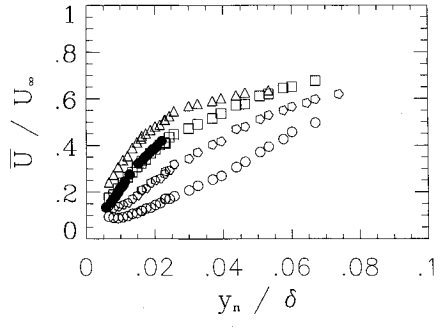

Fig. 5 Comparison of mean streamwise velocity distribution above smooth surface with distributions along lines 1–4 above riblet surface. Symbols as in Figs. 1 and 4.

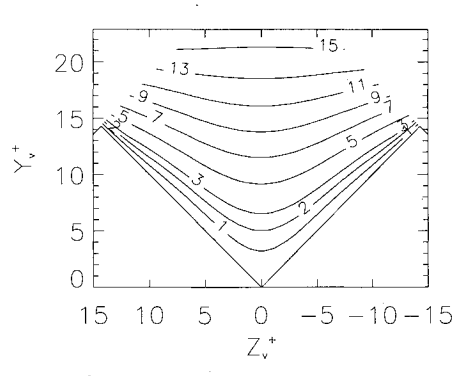

Fig. 6 Contours of constant mean streamwise velocity, normalized by the riblet average friction velocity, $\bar{u}_{\tau_r}$.

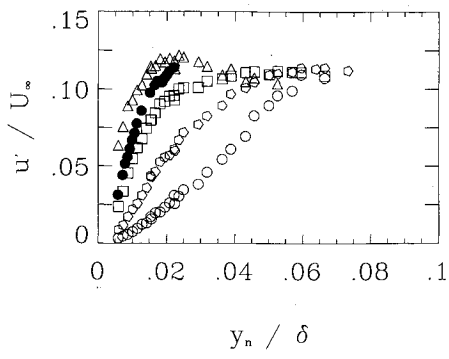

Fig. 7 Comparison of rms streamwise velocity fluctuation intensity distribution above smooth surface with distributions along lines 1–4 above riblet surface. Symbols as in Figs. 1 and 4.

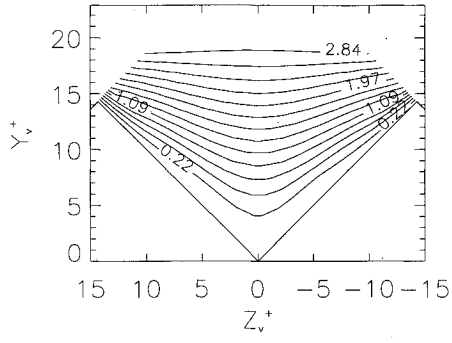

Fig. 8 Contours of constant rms streamwise velocity fluctuations, normalized by the riblet average friction velocity, $\bar{u}_{\tau_r}$.

Results

Single-Sensor Probe Measurements

Instantaneous Time Series Signal

Figure 3 shows samples of the instantaneous streamwise velocity $U(t)$ at a) $y_n/\delta \sim 0.004$ (first location above the wall) and b) 0.011 (sixth location) on the four measurement lines normal to the sidewall of a riblet groove and above the smooth surface. The amplitudes of the fluctuations in the signals become smaller as the riblet valley is approached, very nearly vanishing on line 4 at these locations. The amplitudes of the signal fluctuations in the data sample for the smooth surface at both positions are very similar to those somewhere between lines 1 and 2. These observations will help explain the measured statistical properties discussed later.

Mean Velocity Profiles

Measurements were performed over the smooth surface, for comparison to the riblet surface results. They were also made to determine the accuracy with which such data could be obtained within the very low speed flow of the viscous sublayer, since measurements are rarely attempted there for a boundary layer in air. Figure 4 shows the mean velocity variation within the smooth surface viscous sublayer and buffer layer, scaled with the friction velocity u_τ and the kinematic viscosity ν. The friction velocity was obtained from a least-squares fit of the points below the estimated height of the sublayer (y = 2 mm), not using in the fit the first point, which was obviously influenced by proximity to the wall. All of the data were corrected by a 0.2-mm vertical position shift to meet the no-slip wall condition. This systematic error was presumably due to a combination of positioning inaccuracy and excess acceleration of the flow through the prongs when the probe is

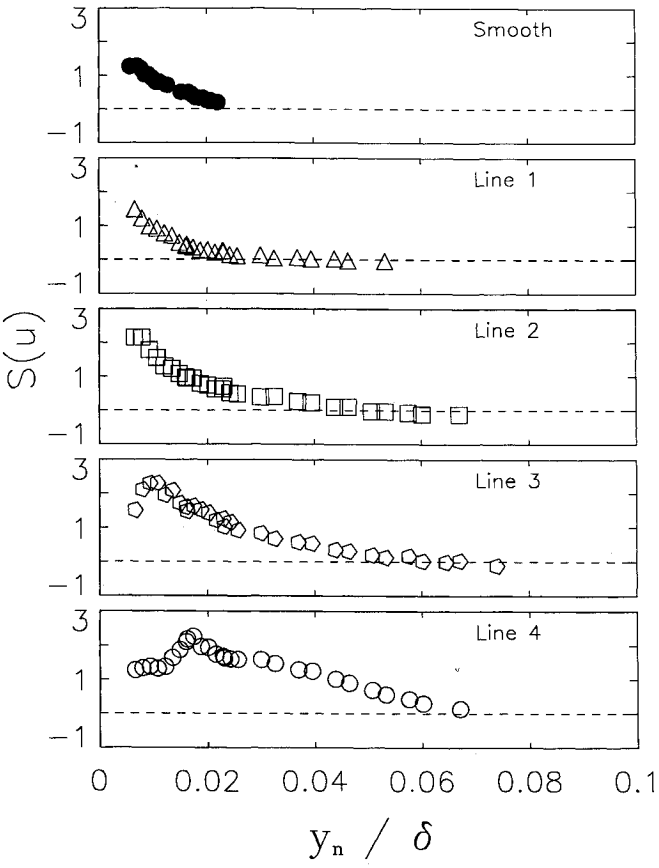

Fig. 9 Skewness factor distributions along lines 1–4.

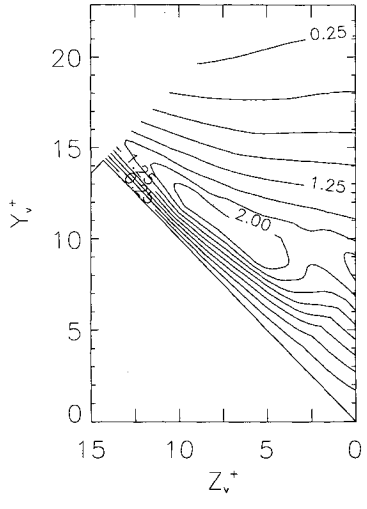

Fig. 10 Contours of constant skewness factor in riblet cross-stream half-plane.

positioned very near the wall. After this correction, the agreement with the linear law in the viscous sublayer is excellent, except for the point at $y^+ \sim 3$, which is slightly high, indicating the onset of other wall proximity effects as noted earlier.

The riblet surface velocity profiles along lines 1–4, normal to the riblet wall, were also obtained and are shown in Fig. 5, where they are compared with the smooth surface data. The data have been normalized with the freestream velocity U_∞ and the boundary-layer thickness δ. The excessively large mean velocities in Fig. 5, for the locations along lines 3 and 4 very close to the wall in the valley, are due to wall proximity effects. Vukoslavčević et al.[3] also showed data that deviated from linearity near the wall because of these wall effects, even when a very low overheat ratio is used.

To decide which data points were affected by the wall and thus not usable to obtain the slope $\partial\bar{U}/\partial y$ for each line, all of the data on each line, including the zero value at the wall, were fitted by a high-order polynomial. By systematically discarding the measured values near the surface until a minimum least-squares error was obtained, the coefficients for each polynomial were found. When these wall proximity affected points were removed, the slope passed through the origin within the acceptable positioning accuracy, which was then corrected. The wall slope of the velocity profile was then obtained by evaluating, at the wall, the differentiated polynomial fitted to the remaining data.

The region within the riblet groove was subsequently evenly spaced in the y_n and z_l directions of Fig. 1, and the velocity values were evaluated at each node of this grid using the polynomials on lines 1–4 and interpolating between these lines. Additional high-

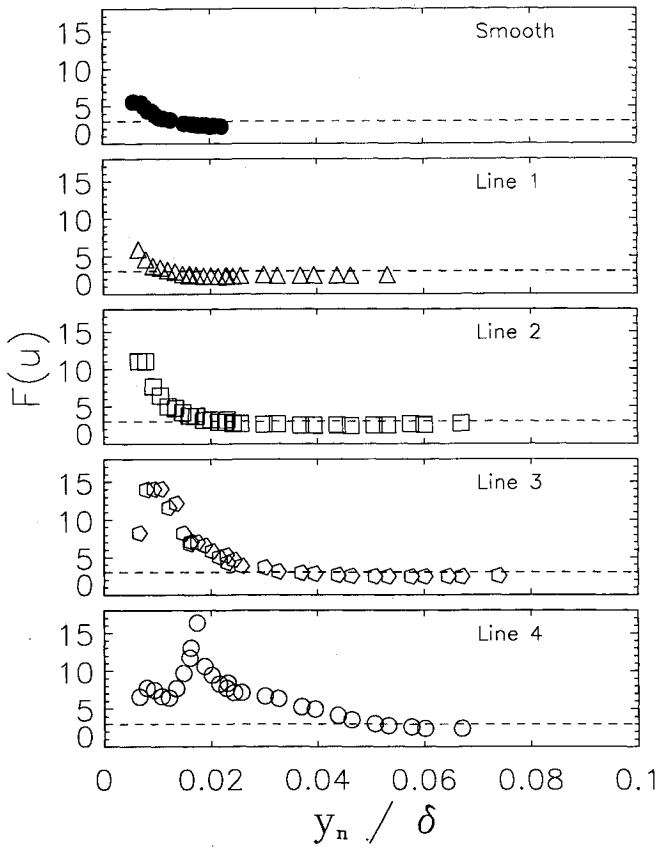

Fig. 11 Flatness factor distributions along lines 1-4.

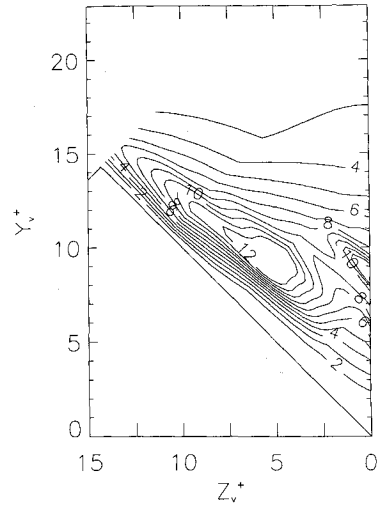

Fig. 12 Contours of flatness factor in riblet cross-stream half-plane.

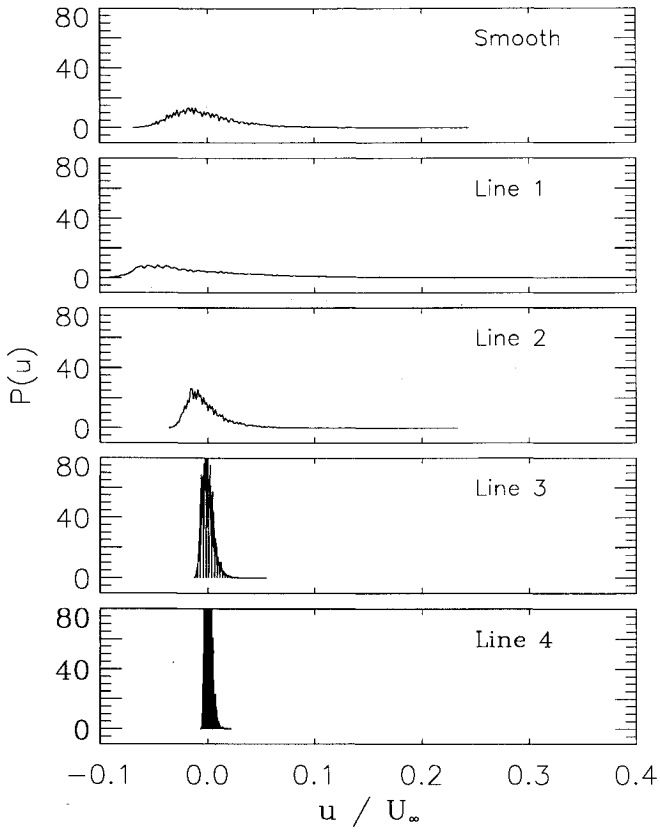

Fig. 13 Comparison of the measured probability density functions of the streamwise fluctuating velocity at $y_n/\delta \approx 0.004$ above the smooth and riblet surfaces.

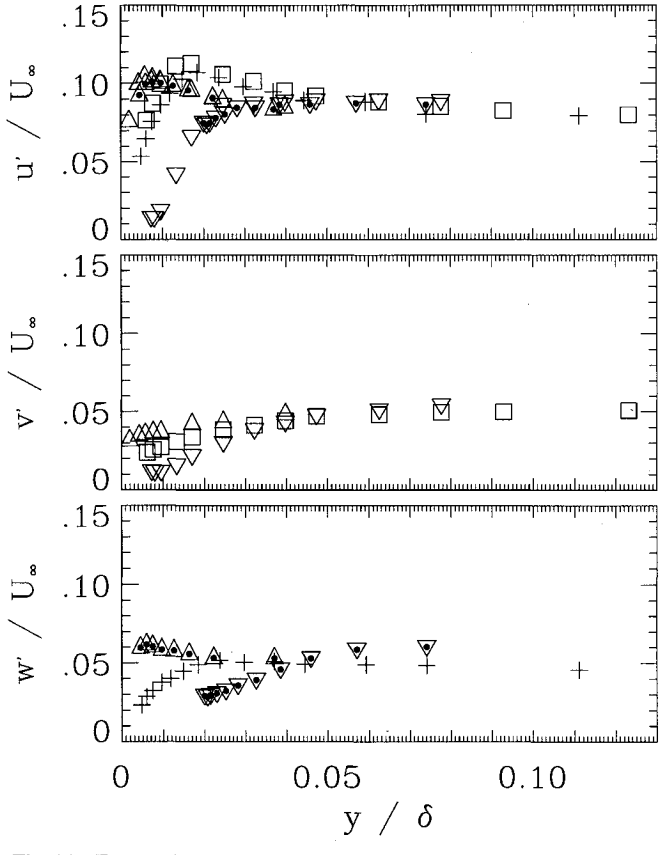

Fig. 14 Fluctuating velocity component turbulence intensity distributions obtained with square-shaped and cross-shaped four-sensor probes. Symbols as in Fig. 2 for the riblet surface and with □ for the square-shaped and + for the cross-shaped four-sensor probes for the smooth surface.

order polynomials were then fitted to the values on the grid lines normal to the surface and between the original lines of data (1–4). Finally, the slope at the wall was obtained for each line, yielding an estimate of the local riblet wall shear stress, which was averaged along the z_l direction to obtain the average riblet friction velocity of $\bar{u}_{\tau_r} = 0.046$ m/s. The average riblet wall shear stress corresponded to about 4% drag reduction (with a ±2% estimated error) compared with the smooth surface drag on the same projected area, in good agreement with the early results of Walsh.[7]

In Fig. 5 the mean velocity gradient at the wall near the riblet peak (line 1) is clearly a little larger than the one over the smooth surface, indicating greater local shear stress there. The smooth surface velocity profile is similar to that at the location one-quarter of the distance below the peak (line 2). At positions lower in the valley (lines 3 and 4), mean velocity gradients at the wall are much smaller than the smooth surface value, indicating the large reduction in local shear stress deep within the riblet valley. The reason for this reduction will be discussed later. The local shear stress must, in fact, go to zero at the very bottom of the riblet valley because of the no-slip condition on the opposite riblet sidewall.

Contours of constant mean velocity inside a single riblet groove were obtained, using the symmetrical geometry of the riblet and the no-slip boundary condition. From these contours, shown in Fig. 6 where they are normalized with $\bar{u}_{\tau_r}$, one sees more clearly the velocity distribution in the riblet groove from the valley to the peak. The mean velocity in the valley, at a fixed y_n position normal to the riblet wall, is greatly reduced compared with the locations near the peak and necessarily goes to zero at the opposite riblet sidewall. The contour closest to the riblet surface has a velocity of only about 5 cm/s, demonstrating the difficulty of the measurements. The spanwise variation of the mean velocity is negligible above $y_v^+ \approx 20$, in very good agreement with the results of Hooshmand et al.[11] The horizontal and vertical dimensions in this figure and in Figs. 8, 10, and 12 are referenced to the riblet valley, denoted by the subscript v, and are made nondimensional with $\bar{u}_{\tau_r}$ and ν.

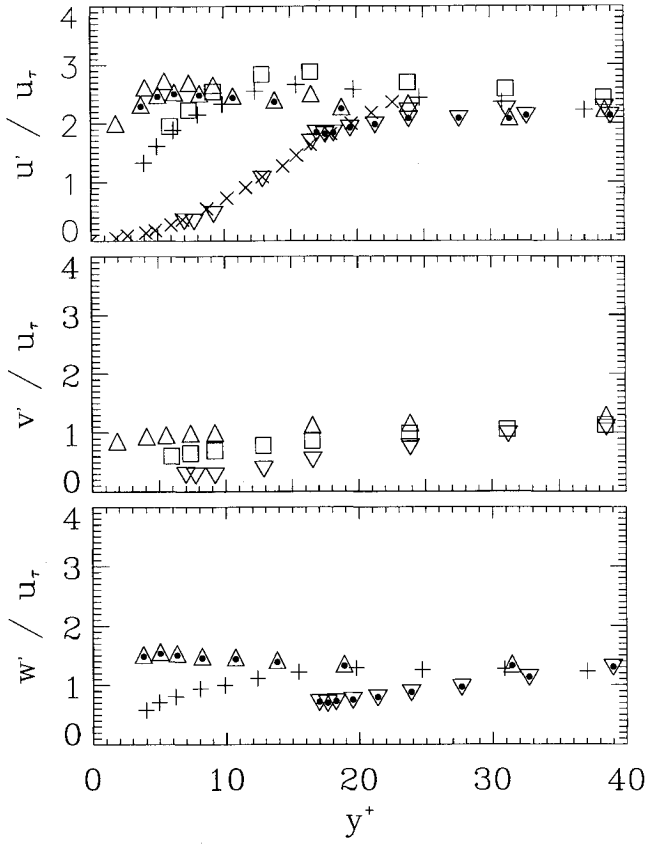

Fig. 15 Fluctuating velocity component rms values normalized with the smooth surface friction velocity u_τ. Symbols as in Fig. 14, and with x indicating single-sensor probe values obtained from the streamwise velocity fluctuation rms contours of Fig. 8 above the valley.

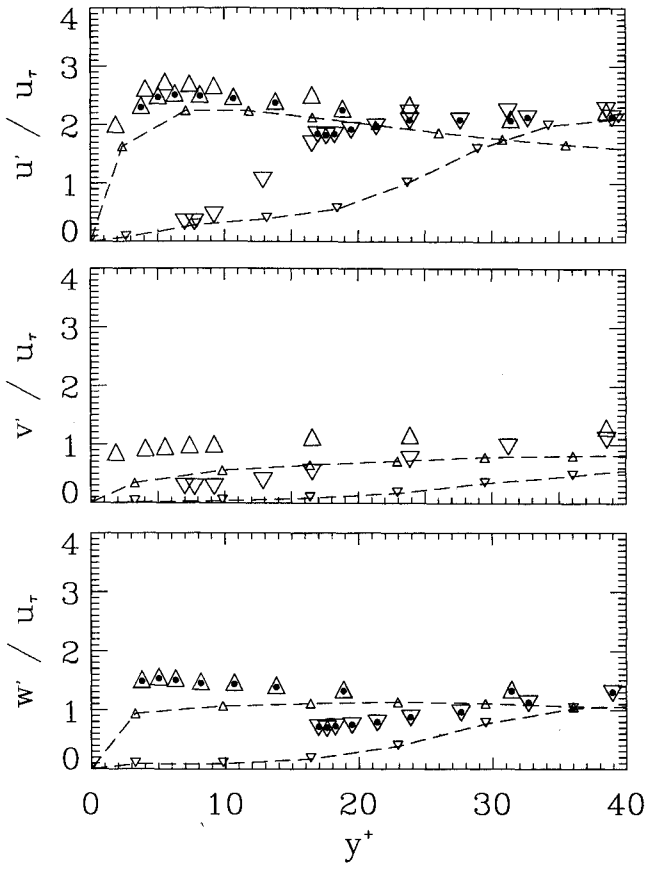

Fig. 16 Peak and valley data of four-sensor probes from Fig. 15 compared with the 60-deg riblet direct numerical simulation results of Chu et al.[4] at $R_\tau = 1.31 \times 10^2$ with $s^+ = 17.1$ (peak, – – Δ – –; valley, – – ∇ – –).

Turbulence Intensities

The distribution of measured rms streamwise fluctuation velocity values u' across the buffer and sublayers for the smooth surface flow are shown in Fig. 7, normalized by U_∞ and δ. These are compared with the values obtained along lines 1-4 normal to the riblet sidewall. It is quite evident that the turbulence intensity increases with distance up the riblet wall from the valley toward the peak at a fixed distance, y_n/δ, above the surface. For example, at 2% of the boundary thickness, the streamwise turbulence intensity near the valley on line 4 drops to 2% of U_∞, whereas at the peak on line 1 for the same y_n/δ, the rms. is six times larger. Vukslavčević et al.[3] observed a similar trend in measurements along the vertical planes of symmetry above the peak and valley. The turbulence intensity of the streamwise fluctuations is reduced compared with the smooth surface values, for fixed y_n/δ, within more than the lower three-quarters of the groove.

Contours of constant rms streamwise velocity fluctuation u' within the riblet, normalized by $\bar{u}_{\tau_r}$, are shown in Fig. 8. Similar to the influence on the mean velocity contours, the effect of the riblets on the rms values of the fluctuations is bounded by $y_v^+ \approx 18$. It is quite apparent that the fluctuations drop to very low levels deep in the riblet groove.

Higher Moments

The normalized higher moments of the streamwise fluctuating velocity component, i.e., the skewness and flatness factors, were obtained. Skewness and flatness factor distributions above the smooth surface and along line 1 are similar, as seen in Figs. 9 and 11. Deeper in the riblet groove, the maximum values are much greater than the smooth surface values for fixed y_n/δ a little less than 0.02. Contours of constant skewness factor are shown in Fig. 10 for the riblet cross-stream half-plane. They show that the peak values of the skewness factor are located in the region between line 2 and line 3 above the wall, as well as on the plane of symmetry at about the midpoint above the valley. These conclusions conform with and extend those of Vukslavčević et al.[3]

Like the skewness, for y_n/δ a little less than 0.02, the flatness factor increases as the valley is approached as seen in Fig. 11. In Fig. 12, contours of the constant flatness factor are shown within the cross-stream half-plane of the riblet. The maximum values of these contour plots occur near the maximum values in the skewness contour plots. When combined with the small turbulence intensity in these regions, as shown in Fig. 8, the large values of skewness and flatness indicate that, occasionally, wallward-directed fluid with large-amplitude, positive, streamwise fluctuations penetrates to just above the midlevel of the riblet at $y_v^+ \approx 10$, but seldom reaches much deeper into the valley.

Probability Density Functions

Probability density functions (PDFs) of the streamwise velocity fluctuations u were determined for the smooth surface and the four different spanwise locations on the riblet surface. Figure 13 shows PDFs for $y_n/\delta \sim 0.004$ on each of the lines 1-4 and above the smooth surface. The PDFs of the streamwise velocity fluctuations, although remaining asymmetric, become very narrow when the location is at the riblet midlevel or below. This further confirms the observation that the high-speed wallward-directed fluid seldom penetrates below $y_v^+ \approx 10$ while still retaining much streamwise momentum.

Four-Sensor Probe Measurements

Turbulence Intensity Measurements

In Fig. 14 turbulence intensity distributions are shown for all three components of the velocity vector above the smooth surface and along the vertical lines of symmetry above the riblet peak and valley, normalized with U_∞ and δ. The values of u' and v' were measured with the square-shaped probe and of u' and w' with the cross-shaped probe. Two observations can be made. First, the values of u' from each of the respective probes agree rather well with

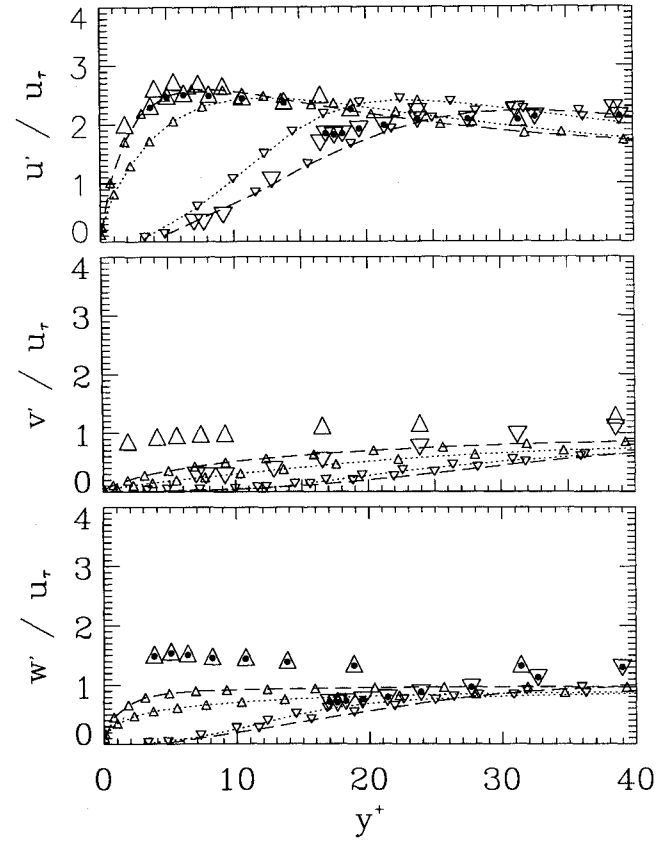

Fig. 17 Peak and valley data of four-sensor probes from Fig. 15 compared with the 45-deg riblet direct numerical simulation results of Choi et al.[5] at $R_\tau = 1.80 \times 10^2$ with $s^+ = 16.4$ (peak, ··· Δ ···; valley, ··· ∇ ···) and $s^+ = 32.8$ (peak, – – Δ – –; valley, – – ∇ – –).

each other for both smooth and riblet surfaces. Second, all three components show significantly higher intensities over the peak and lower intensities over the valley, as the surface is approached, compared with the smooth surface values. This latter observation for u' agrees with the single-sensor probe measurements discussed earlier but also shows that the cross-stream components are affected similarly to the streamwise components.

To compare our results with the simulation results of Chu et al.[4] and Choi et al.,[5] our laboratory data in Fig. 14 is replotted in Fig. 15 and normalized with the smooth surface friction velocity u_τ, and ν. This scaling is necessary for the comparison because the differences between the channel flow simulations and the boundary-layer experiment make U_∞ and δ inappropriate scales, and the riblet surface friction velocity $\bar{u}_{\tau_r}$ was not accurately determined in the four-sensor probe experiments. The trends observed in Fig. 14 are also observed here with this scaling. Included are the renormalized single-sensor probe values of u' taken along the vertical plane of symmetry above the valley from the contour values of Fig. 8; they agree very well with the four-sensor probe data. Our peak and valley rms data from Fig. 15 are compared with those from the simulation of Chu et al.[4] in Fig. 16. Although the trends of the data, i.e., higher rms values over the peak and lower values over the valley, are the same for all three components, their values have smaller magnitudes than ours, particularly in the valley. It should be noted, however, that their triangular riblet geometry is one with the walls forming a 60-deg angle with the horizontal, i.e., with $h^+ = s^+ = 17.1$, based on the riblet average friction velocity. In addition, our three experimental Reynolds numbers R_τ were, respectively, 3.8, 6.4, and 7.4 times greater than their value of 1.31 $\times 10^2$. In Fig. 17 our peak and valley data from Fig. 15 are compared with two cases of Choi et al.[5] Both cases are for 45-deg riblets, but in case A $h^+ = 16.4$ and $s^+ = 32.8$, based on the riblet surface average friction velocity, whereas in case C these dimensions are $h^+ = 8.2$ and $s^+ = 16.4$. Our three experimental Reynolds numbers R_τ were respectively, 2.8, 4.6, and 5.4 times greater than their value of 1.8×10^2. They found that case C with the smaller riblets gave a 5% drag reduction, but case A gave a 2% drag increase. Our riblet dimensions for the single-sensor probe measurements are a

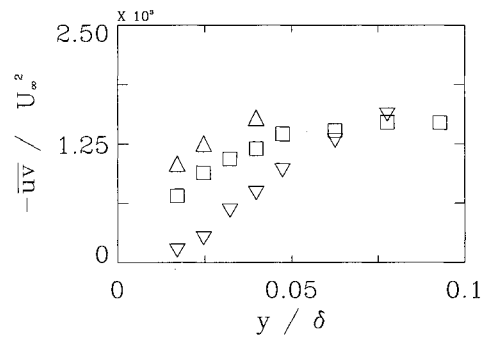

Fig. 18 Distributions of Reynolds shear stress, normalized with the freestream velocity and obtained with the square-shaped four-sensor probe, near the smooth surface (□), above the riblet peak (△), and above the riblet valley (▽).

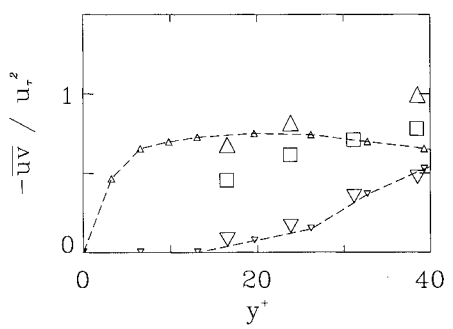

Fig. 19 Reynolds shear stress experimental data from Fig. 18 compared with the peak and valley simulation results of Chu et al.[4] at R_τ = 1.31 $\times 10^2$, with $s^+ = 17.1$ (peak, −− △ −−; valley, −− ▽ −−).

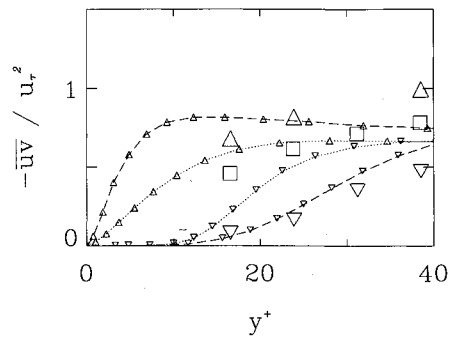

Fig. 20 Reynolds shear stress experimental data from Fig. 18 compared with the peak and valley simulation results of Choi et al.[5] at R_τ = 1.8 $\times 10^2$ with $s^+ = 16.4$ (peak, ··· △ ···; valley, ··· ▽ ···) and $s^+ = 32.8$ (peak, −− △ −−; valley, −− ▽ −−).

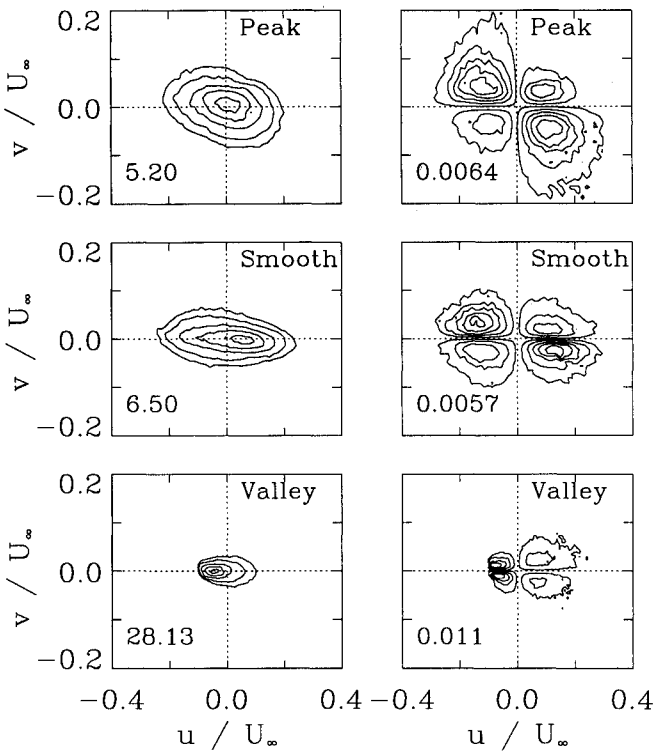

Fig. 21 Constant a) joint probability density functions and b) covariance integrand contours of the u and v fluctuations at $y/\delta \sim 0.015$ above the smooth and riblet surfaces.

little smaller than their drag-increasing case A and considerably larger than their drag-reducing case C. Our dimensions for the measurements with the four-sensor probes were quite a bit larger than their drag-increasing case A. Our u' values, for both peak and valley, are in quite good agreement with their larger (case A) riblet values. The trends of our peak and valley v' and w' values are similar to theirs, but our magnitudes are higher. This could be due to several factors. These variables, scaled in this manner, are quite dependent on Reynolds number for low Reynolds number. Also, Park[9] has shown that the four-sensor probes overestimate the values of v' and, to a lesser degree, w'. In spite of the lack of complete agreement between the experiment and the simulations, it is quite evident that all three components of velocity have reduced rms values in the valley of the riblet and increased values over the peak compared with the smooth surface values.

Reynolds Shear Stress Measurements

The distributions of the experimentally measured Reynolds shear stress, normalized with U_∞^2 and plotted vs y/δ, are shown in Fig. 18, for the symmetry planes above the peak and valley of the

riblet surface and above the smooth surface. The data for $y^+/\delta < 0.02$ are not shown because the errors were considered too large in that region. In spite of this limitation, it is evident that the Reynolds shear stress in the valley is substantially reduced compared with the smooth surface values, approaching negligibly small values near the riblet midlevel. Over the peak the Reynolds shear stress is larger than the smooth surface value. The peak and valley results from Chu et al.[4] and the two cases of Choi et al.[5] are compared with these data, normalized with u_τ^2, in Figs. 19 and 20. The trends and, in general, the magnitudes are similar even though there are some differences in detail. One obvious difference in the experiment and simulations with regard to Reynolds shear stress values, in addition to those mentioned earlier, is the fact that the channel flow, unlike the boundary layer, has no constant stress region.

Joint Probability Density Function and Covariance Integrand

The joint probability density functions (JPDFs) of the streamwise and vertical velocity fluctuations u and v are shown in Fig. 21a, for $y/\delta \approx 0.015$ above the riblet valley and peak and above the smooth surface. The diminished correlation in the valley is strikingly evident as well as the substantially higher probability of the flow at this location to have u values less than the local mean. This is consistent with the positive skewness shown in Fig. 10 and indicates that higher momentum fluid from above rarely penetrates this deep into the riblet valley. The covariance integrands, $uvP(u, v)$, shown in Fig. 21b, where

$$\overline{uv} = \int_{-\infty}^{+\infty}\int_{-\infty}^{+\infty} uvP(u, v)\, du\, dv$$

makes these conclusions even more evident. Whereas the contribution to the covariance, $\overline{uv}$, comes primarily from quadrants 2 and 4 above the smooth surface and prounouncedly so above the peak at this y/δ location, the picture is dramatically changed deep in the valley. Here quadrants 2 and 3 (negative u) are highly probable, but quadrants 1 and 4 are broader, indicating occasional higher amplitude positive u fluid motions.

Conclusions

For riblets of a dimensionless size within the drag reducing range, the following conclusions can be made:

1) The mean velocity is greatly retarded, along lines parallel to a riblet sidewall, as the riblet valley is approached.

2) The mean shear stress at the riblet wall, τ_w, at about one-quarter of the riblet sidewall below the peak is about the same as that on a smooth surface with the same freestream velocity for the conditions studied here. Thus, about three-quarters of the riblet sidewall experiences a mean shear stress less than the smooth surface value, resulting in net drag reduction.

3) The rms streamwise turbulence intensity is greatly diminished along lines parallel to the riblet sidewall with distance into the valley. Deep within the riblet groove the flow is in an almost laminar state.

4) The turbulence intensities of all three velocity components, along vertical lines of symmetry, are diminished over the valley and increased over the peak of the riblet surface compared with the smooth surface intensities.

5) Vertical flux of streamwise momentum is greatly reduced within the riblet, even for a dimensionless size somewhat above the drag-reducing range. High-momentum fluid from layers above the riblet rarely penetrate into the lower half of the riblet groove.

Acknowledgments

This research was supported by the National Science Foundation under Grant 891189. The four-sensor probe used was built by P. Vukoslavčević who, along with B. Marasli, gave us many helpful suggestions during the course of this work.

References

[1]Walsh, M. J., "Riblets as a Viscous Drag Reduction Technique," *AIAA Journal*, Vol. 21, No. 4, 1983, pp. 485, 486.

[2]Bechert, D. W., and Bartenwerfer, M., "The Viscous Flow on Surfaces with Longitudinal Ribs," *Journal of Fluid Mechanics,* Vol. 206, Sept. 1989, pp. 105–129.

[3]Vukoslavčević, P., Wallace, J. M., and Balint, J.-L., "Viscous Drag Reduction Using Streamwise-Aligned Riblets," *AIAA Journal,* Vol. 30, No. 4, 1992, pp. 1119–1122.

[4]Chu, D., Henderson, R., and Karniadakis, G. E., "Parallel Spectral Element-Fourier Simulation of Turbulent Flow over Riblet Mounted Surface," *Theoretical and Computational Fluid Dynamics,* Vol. 3, March 1992, pp. 219–229.

[5]Choi, H., Moin, P., and Kim, J., "Direct Numerical Simulation of Turbulent Flow over Riblets," NASA Ames Research Center, CTR Manuscript 137, July 1992.

[6]Blackwelder, R. F., and Haritonidis, J. H., "Scaling of the Bursting Frequency in Turbulent Boundary Layers," *Journal of Fluid Mechanics,* Vol. 132, July 1983, pp. 87–103.

[7]Walsh, M. J., "Drag Characteristics of V-Groove and Transverse Curvature Riblets," *Viscous Drag Reduction,* edited by G. R. Hough, Vol. 72, Progress in Astronautics and Aeronautics, AIAA, New York, 1980, pp. 168–184.

[8]Walsh, M. J., "Turbulent Boundary Layer Drag Reduction Using Riblets," AIAA Paper 82-0169, Jan. 1982.

[9]Park, S.-R., "An Experimental Study of Passive Drag Reduction in a Turbulent Boundary Layer by a Riblet Surface," Ph.D. Dissertation, Univ. of Maryland, Dept. of Mechanical Engineering, College Park, MD, 1992.

[10]Vukoslavčević, P., and Wallace, J. M., "Influence of Velocity Gradients on Measurements of Velocity and Streamwise Vorticity with Hot-Wire X-Array Probes," *Review of Scientific Instruments,* Vol. 52, No. 6, June 1981, pp. 869–879.

[11]Hooshmand, A., Youngs, R. A., and Wallace, J. M., "An Experimental Study of Changes in the Structure of a Turbulent Boundary Layer due to Geometry Changes," AIAA Paper 83-0230, Jan. 1983.